Nanoscale Res Lett (2007) 2:81–86
DOI 10.1007/s11671-006-9034-4

NANO EXPRESS

Synthesis, structure and magnetic properties of β-MnO_2 nanorods

Hae Jin Kim · Jin Bae Lee · Young-Min Kim · Myung-Hwa Jung · Z. Jagličić · P. Umek · J. Dolinšek

Published online: 11 January 2007

Abstract We present synthesis, structure and magnetic properties of structurally well-ordered single-crystalline β-MnO_2 nanorods of 50–100 nm diameter and several μm length. Thorough structural characterization shows that the basic β-MnO_2 material is covered by a thin surface layer (~2.5 nm) of α-Mn_2O_3 phase with a reduced Mn valence that adds its own magnetic signal to the total magnetization of the β-MnO_2 nanorods. The relatively complicated temperature-dependent magnetism of the nanorods can be explained in terms of a superposition of bulk magnetic properties of spatially segregated β-MnO_2 and α-Mn_2O_3 constituent phases and the soft ferromagnetism of the thin interface layer between these two phases.

Keywords Self-assembled nanorods · Manganese oxides · Nanoscale magnetism

H. J. Kim · J. B. Lee
Energy Nano Material Team, Korea Basic Science Institute, Daejeon 305-806, Korea

Y.-M. Kim
Division of Electron Microscopic Research, Korea Basic Science Institute, Daejeon 305-806, Korea

M.-H. Jung
Quantum Material Research Team, Korea Basic Science Institute, Daejeon 305-806, Korea

Z. Jagličić
Institute of Mathematics, Physics and Mechanics, Jadranska 19, Ljubljana 1000, Slovenia

P. Umek · J. Dolinšek (✉)
J. Stefan Institute, University of Ljubljana, Jamova 39, Ljubljana 1000, Slovenia
e-mail: jani.dolinsek@ijs.si

Introduction

The one-dimensional (1D) nanostructures in the form of single-crystalline nanorods and nanowires have attracted considerable interest because of their fascinating application as interconnects and building blocks in the nanoscale electronic, optoelectronic, and spintronic devices [1–3]. Self-assembled quasi-1D nanorods and nanowires, of typically several 10 nm in diameter and several μm in length, are the smallest-dimension structures that still allow efficient transport of electrons. The nanorod- and nanowire form of the material is considered to influence its physical properties, which depart from the properties of their bulk phases due to quantum effects related to the shape and size [4]. These effects represent a key factor to the ultimate performance and application of the nano-sized material.

Among several known materials that can be efficiently prepared in the nanorod/nanowire form, manganese oxides are of considerable importance in technological applications such as catalysis, molecular sieves and electrodes in rechargeable batteries, owing to their outstanding structural flexibility combined with novel chemical and physical properties [5]. Out of the many polymorphic forms of manganese dioxide (α, β, γ and δ), which involve different linking of the basic-unit [MnO_6] octahedra, α-MnO_2 nanowires have been successfully synthesized by the acidification–hydrothermal method [6], whereas their subsequent treatment with ethanol resulted in γ-Mn_2O_3 nanowire bundles. Single-crystalline nanowires of α- and β-MnO_2 were also prepared by selected-control hydrothermal method [7] through the oxidation of Mn^{2+} by $S_2O_8^{2-}$ in the absence of catalysts or templates. A mixture of

single-crystalline cubic MnO and tetragonal Mn_3O_4 nanowires was reported to be the final product of a synthesis involving thermal evaporation of $MnCl_2$ under argon flow, and the nanowires showed unusual magnetic properties [8] (i.e., the MnO nanowires appeared ferromagnetic (FM) with $T_C = 12$ K, though bulk MnO is antiferromagnetic, AFM). In this paper we present a hydrothermal method for the synthesis of single-crystalline β-MnO_2 nanorods of excellent structural quality. We examine phase purity of the nanorods and show that structurally well-ordered β-MnO_2 material is covered by a thin (~2.5 nm) surface layer of α-Mn_2O_3 phase with a reduced Mn valence state. We also present magnetic properties of the β-MnO_2 nanorods and demonstrate the important role of the surface layer in the rich temperature-dependent magnetism of this material.

Synthesis and characterization

The synthesis of the β-MnO_2 nanorods involved LiOH, $Mn(NO_3)_2 \times H_2O$ and citric acid in a molar ratio 1.2:2:3.2 as the starting compounds, which were dissolved in water and the polymer poly(ethylene glycol)–block–poly(propylene glycol)–(1100) was added. The mixture was stirred in a magnetic field of 0.6 T strength and then 50 ml of the solution was sealed in an 80 ml teflon-lined autoclave. Hydrothermal synthesis was performed at 100 °C for 48 h. The product was filtered and rinsed with ethanol and dried at 100 °C for 12 h. The polymer involved in the synthesis was fired out by sintering at 500 °C in air for 2 h, which resulted in a black solid as the final product. The role of the polymer in the synthesis and the calcination of the polymeric precursor at high temperature in air are described elsewhere [9], whereas the chemistry of manganese citrate complexes is explained in [10]. Scanning electron- (SEM) and transmission electron (TEM) microscope images of the product material (Fig. 1) show its morphology in the form of nanorods of dimensions 50–100 nm in diameter and 1–3 μm in length. SEM image (Fig. 1a) also reveals that the nanorods were synthesized with a high yield.

The x-ray spectra revealed the presence of two phases (Fig. 2). The majority phase is the β-MnO_2 pyrolusite tetragonal structure with $a = 4.40410$ Å, $c = 2.87650$ Å and space group $P4_2/mnm$, whereas the minority phase could be indexed to the α-Mn_2O_3 bixbyte orthorhombic structure with $a = 9.41610$ Å, $b = 9.42370$ Å, $c = 9.40510$ Å and space group $Pcab$. The relation of the two phases becomes evident from the high-resolution (HRTEM) image of a single

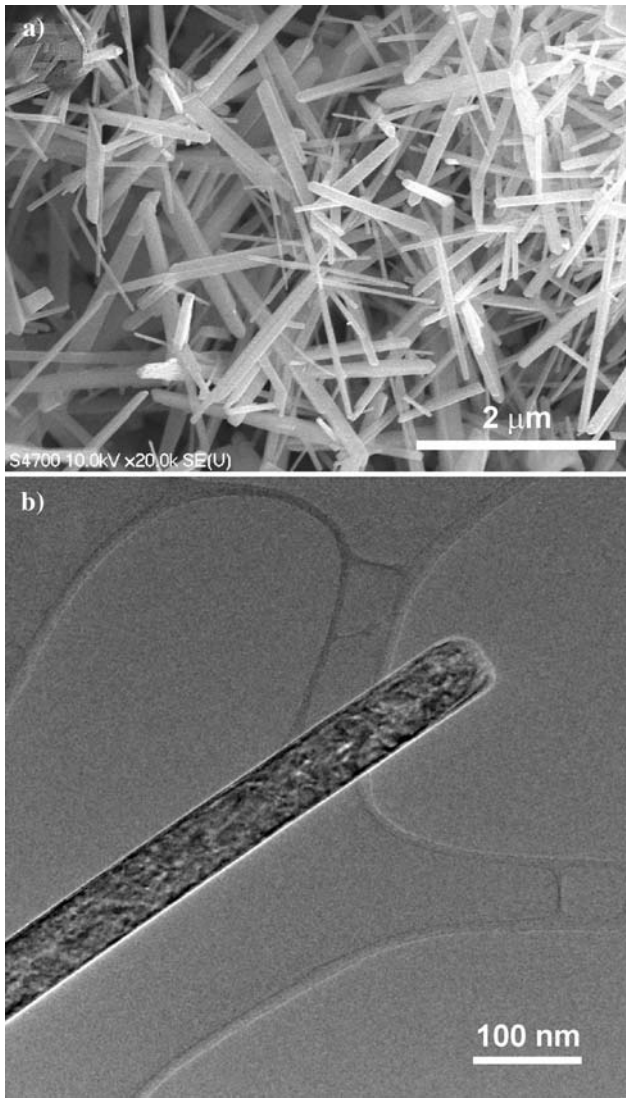

Fig. 1 (**a**) SEM image of β-MnO_2 nanorods and (**b**) TEM image of a single nanorod

nanorod (Fig. 3a) that was acquired using JEOL JEM–ARM1300S high-voltage electron microscope (operated at 1250 kV) with 1.2 Å point–point resolution. It is observed that the interior of the selected nanorod of 70 nm diameter consists of well-ordered crystalline material, which is at the surface covered by a 2.5-nm thin layer of another crystalline phase. The electron diffraction patterns in Fig. 3a confirm that the interior of the nanorod is the β-MnO_2 phase, whereas the surface layer is the α-Mn_2O_3 phase, in agreement with the x-ray analysis of Fig. 2. The manganese in the β-MnO_2 phase is in a Mn^{4+} state, whereas its valence is reduced to Mn^{3+} in the α-Mn_2O_3 surface layer, so that the environment (very likely carbon coating during firing procedure in air) obviously acts as a reducent to

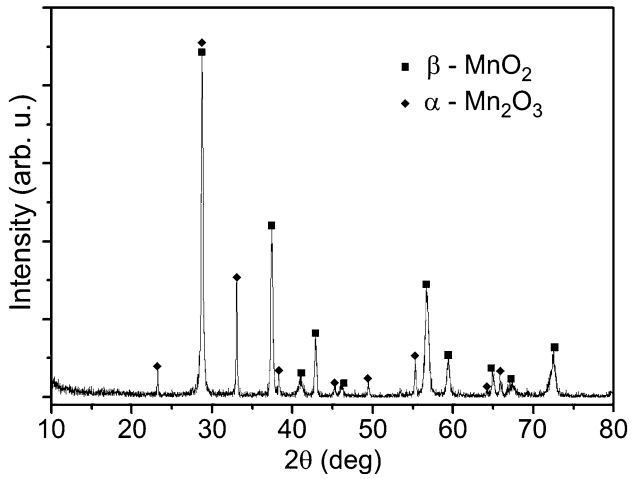

Fig. 2 X-ray diffraction pattern of the β-MnO_2 nanorods. Two sets of peaks are identified, one indexed to the β-MnO_2 pyrolusite phase and the other to the α-Mn_2O_3 bixbyte phase

the manganese in the last step of the synthesis procedure. In Fig. 3b, atomic model of the β-MnO_2 phase (viewed along [1 1 0]) is superimposed on the experimental HRTEM image, showing good matching and confirming single-crystalline form of the nanorod. The β-MnO_2 pyrolusite unit cell is also shown. Here we mention that, despite the two-phase structure of the nanorods, we shall keep labeling them by the generic name "β-MnO_2 nanorods".

Magnetic properties

Magnetic measurements were performed by a Quantum Design SQUID magnetometer equipped with a 5 T magnet and the measurements were conducted between room temperature and 2 K. The $M(H)$ curves at 5, 55 and 110 K are displayed in Fig. 4a, showing linear dependence of the magnetization on the magnetic field with a positive slope up to the highest field 5 T. The $M(H)$ curve at 5 K exhibits small hysteresis around $H = 0$ with a coercivity of 0.9 kOe (shown on an expanded scale in Fig. 4b), demonstrating that the magnetization at this temperature contains a FM component, which is not observed at 55 K and higher. The magnetization as a function of temperature, $M(T)$, in magnetic fields 50 Oe, 100 Oe, 1000 Oe, 1 T and 5 T is displayed in Fig. 5a–e. Both zero-field-cooled (zfc) and field-cooled (fc) runs are shown. Upon cooling from room temperature, the $M(T)$ curves first exhibit two close maxima at temperatures 93 K and 80 K (best observed on the 5 T and 1 T curves) that are independent of the magnetic field, followed by a decrease of

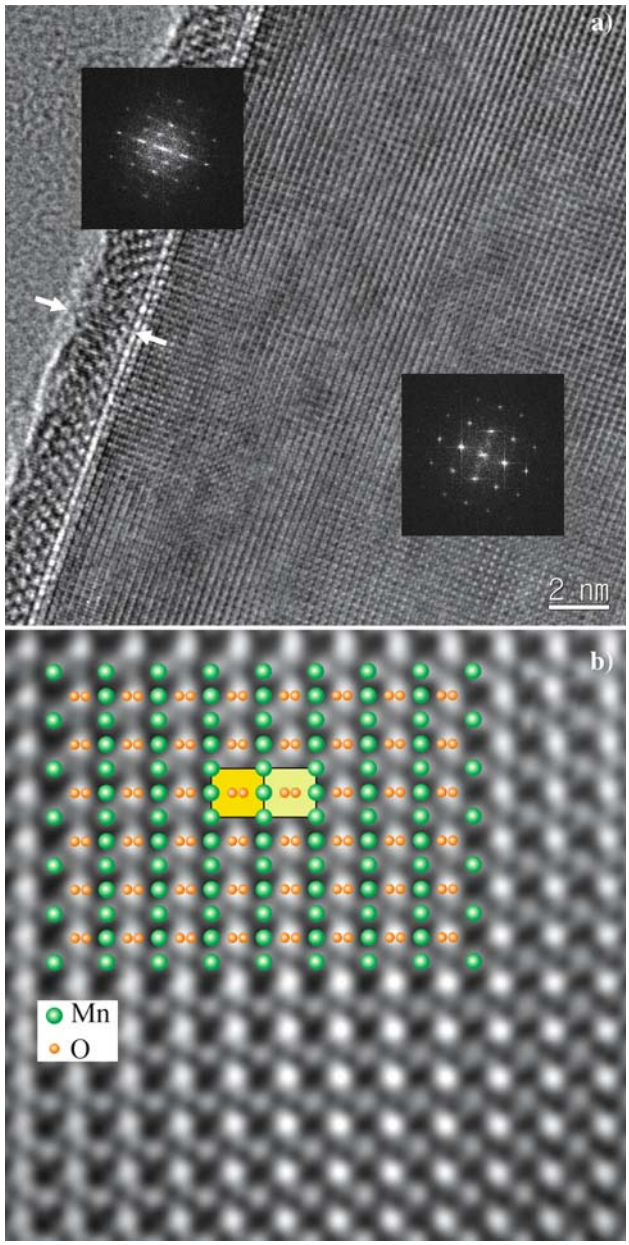

Fig. 3 (Color online) (**a**) Atomic-resolved HRTEM image of a β-MnO_2 nanorod, showing that the β-MnO_2 single-crystalline material in the interior of the rod is covered by a 2.5-nm thin surface layer of the α-Mn_2O_3 phase (located between the two arrows). The electron diffraction patterns of the two phases are also shown. The right arrow points at the interface layer between the β-MnO_2 and the α-Mn_2O_3 phases. In (**b**), atomic model of the β-MnO_2 phase (viewed along [1 1 0]) is superimposed on the experimental HRTEM image of thickness 44 nm and defocus –44 nm (Mn, green (large) circles; O, orange (small) circles). The β-MnO_2 pyrolusite unit cell is also shown

the magnetization. Below the temperature of about 45 K the zfc–fc splitting starts to be observed. The zfc–fc splitting is quite significantly affected by the external magnetic field. In the low-field regime

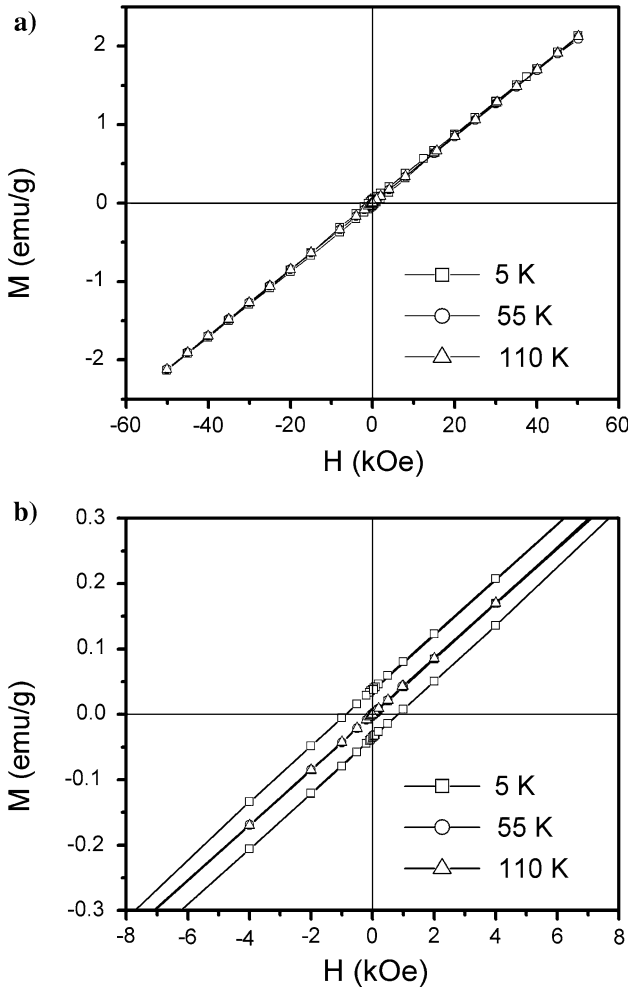

Fig. 4 (**a**) Magnetization as a function of the magnetic field of the β-MnO_2 nanorods at 5, 55 and 110 K. **(b)** Expanded portions of the $M(H)$ curves, showing hysteresis at 5 K

(below 1000 Oe), the zfc–fc splitting increases with the field (at the lowest measuring temperature of 2 K, the splitting in 1000 Oe is three times larger than in 50 Oe), whereas at higher fields, the splitting becomes smaller again, showing tendency to vanish. The zfc–fc curves also show features typical of magnetically unstable systems: (i) the shapes of the zfc and fc curves are strongly affected by the applied field and (ii) in the highest field 5 T, the zfc curve even crosses the fc curve and becomes higher above 30 K. This demonstrates that, within the regime of the zfc–fc splitting, magnetic ordering in the β-MnO_2 nanorods is soft with internal fields of comparable magnitude to the externally applied field. In order to check whether the zfc–fc magnetization splitting is related to a magnetic phase transition, we performed ac magnetization measurements at frequencies 1, 10, 100 and 1000 Hz (Fig. 5f). We observe a frequency-independent peak at 40.5 K, indicating a thermodynamic FM-type phase transition with a critical slowing-down of the spin fluctuations.

Discussion

The rich structure of the $M(T)$ curves can be analyzed by considering magnetic properties of the β-MnO_2 and α-Mn_2O_3 bulk phases. Bulk β-MnO_2 undergoes a transition to an incommensurately-modulated helical AFM state at $T_N \approx 92.5$ K that exhibits both long- and short-range magnetic orders [11, 12]. Its magnetic susceptibility exhibits well-developed peak at T_N [12]. Since β-MnO_2 is also the dominant phase of our investigated nanorods, it is straightforward to attribute the peak in the magnetization at 93 K in Fig. 5 to the same magnetic phase transition. The nanodimensions of the material obviously do not destroy the AFM state of the bulk phase. Regarding magnetic ordering of the α-Mn_2O_3 bulk phase, a neutron study has shown [13] that majority of the magnetic peaks disappear above $T_N \sim 80$ K (a similar transition temperature $T_N \sim 79$ – 80 K was reported also from heat capacity measurements [14] and magnetic susceptibility and Mössbauer effect [15] on $Mn_{2-x}Fe_xO_3$). According to the neutron results [13], magnetic order in the bulk α-Mn_2O_3 can be described by a set of six collinear AFM spin arrangements on a cubic lattice. The peak at 80 K in the $M(T)$ of the investigated β-MnO_2 nanorods can be thus associated with the magnetic ordering within the α-Mn_2O_3 surface layer. Therefore, the two maxima in the $M(T)$ of the nanorods at 93 and 80 K can be given a simple explanation by invoking magnetic properties of the bulk β-MnO_2 and α-Mn_2O_3 phases (in Fig. 5a, the temperatures of the magnetization maxima expected for these two bulk phases are indicated by dashed lines). A surprising effect is the low-temperature FM magnetization component that cannot be attributed to any of these two phases. The ac magnetization peak at 40.5 K suggests that additional manganese-oxide phases could be present in the investigated β-MnO_2 nanorods. The Mn_2O_3 material has two structural isomers: α-Mn_2O_3 is the thermally stable mineral bixbyte, whereas γ-Mn_2O_3 is thermally less stable and does not occur naturally. On heating up to 600–800 °C in air, γ-Mn_2O_3 transforms into the stable α-Mn_2O_3. Recent magnetic measurements on γ-Mn_2O_3 nanoparticles [16] have shown that the nanoparticle-material exhibits ferrimagnetism below $T_C = 39$ K with high coercivity (~8 kOe at 5 K). Similarly, the Mn_3O_4 bulk material (that is isostructural with γ-Mn_2O_3) was reported [17] to undergo a transition to a ferrimagnetic state at $T_C = 42$ K. In another study [18], Mn_3O_4

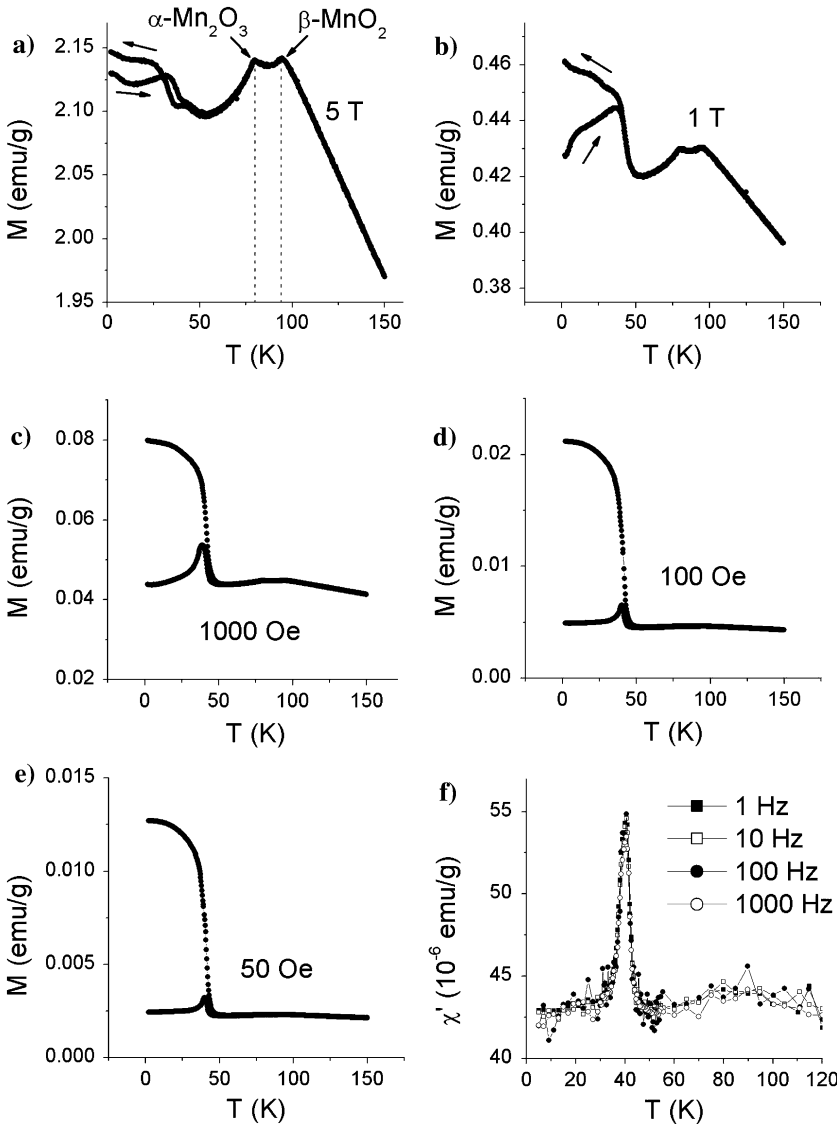

Fig. 5 Magnetization of the β-MnO_2 nanorods as a function of temperature in magnetic fields (**a**) 5 T, (**b**) 1 T, (**c**) 1000 Oe, (**d**) 100 Oe and (**e**) 50 Oe. Both zero-field-cooled (zfc) and field-cooled (fc) runs are shown. Note that the spans of the vertical scale in panels are different. The temperatures of the magnetization maxima expected for the bulk phases of β-MnO_2 (T_N ~ 92.5 K) and α-Mn_2O_3 (T_N ~ 80 K) are indicated in panel (a) by dashed lines. (**f**) ac susceptibility χ' in the field of amplitude 6.5 Oe as a function of temperature at frequencies 1, 10, 100 and 1000 Hz

nanoparticles of varying diameters between 6 and 15 nm showed size-dependent T_C between 36 and 41 K. These FM transition temperatures are remarkably close to that observed in our β-MnO_2 nanorods. However, all the peaks in the x-ray spectrum of the nanorods in Fig. 2 can be indexed to the β-MnO_2 and α-Mn_2O_3 phases and do not reveal the presence of any additional phase within the sensitivity of the XRD experiment (about 2% volume). Careful comparison with the x-ray spectra of the γ-Mn_2O_3 nanoparticles (see Fig. 2 of [16]) and the Mn_3O_4 nanowires (see Fig. 2 of [8]) shows that there are no traces of these two phases in the x-ray spectrum of Fig. 2. The most probable origin of the FM component in the magnetization of the β-MnO_2 nanorods is then magnetic ordering within the mismatch layer at the interface between the β-MnO_2 interior phase and the α-Mn_2O_3 surface layer that can be identified in Fig. 3a unambiguously as two columns of white spots (located at the position of the right arrow). The physics and chemistry of this thin mismatch layer (of thickness about two atomic monolayers) cannot be discussed easily, but there exists reasonable possibility that FM correlations, analogous to those in Mn_3O_4 and γ-Mn_2O_3 phases, could develop between the Mn spins within the interface layer. The small magnetization coercivitiy of 0.9 kOe at 5 K of the β-MnO_2 nanorods (Fig. 4b) does not, however, support direct analogy with neither the γ-Mn_2O_3 nanoparticle-material nor the Mn_3O_4, which are both characterized by high coercivities of the order 8 kOe [16, 17, 19]. The FM spin structure within the investigated β-MnO_2 nanorods is obviously much softer.

The relatively complicated temperature-dependent magnetism of the investigated β-MnO_2 nanorods can, therefore, be explained in terms of a superposition of

magnetic properties of the spatially segregated constituent manganese-oxide phases β-MnO_2 and α-Mn_2O_3, whereas the FM component is most likely associated with the not-well-understood magnetism of the mismatch layer at the interface between these two phases. The interior β-MnO_2 phase and the α-Mn_2O_3 thin surface layer both exhibit AFM properties analogous to their bulk phases (the temperatures of the maxima in the T-dependent magnetization of the nanorods and the bulk materials match well) despite the nanodimensions of the rods. These results show how important it is to make a thorough structural characterization of the material on the atomic-resolution scale before entering the discussion on the influence of nanodimensions on the physical properties of the material. We should also like to mention that similar structure of a thin surface layer of another phase that covers the basic β-MnO_2 material was observed (see Fig. 3d of [7]), though not discussed, also for the β-MnO_2 nanorods produced by the selected-control hydrothermal synthesis [7], so that this kind of structure of the β-MnO_2 nanorods seems to appear quite commonly.

Conclusions

To summarize, we presented a hydrothermal method for the synthesis of structurally well-ordered single-crystalline β-MnO_2 nanorods. We show that the basic β-MnO_2 material is covered by a thin surface layer of the α-Mn_2O_3 phase with a reduced Mn valence that adds its own magnetic signal to the total magnetization. The nanodimensions of the investigated nanorods do not appear to affect significantly their magnetic response, which can be explained as a superposition of bulk magnetic properties of the spatially segregated constituent manganese-oxide phases and the magnetism of the thin interface between them. This result prompts for further investigations of the magnetism of nano-sized materials in order to prove/disprove the often-claimed exceptionality of magnetism on the nanometric scale.

Acknowledgment This work was supported by the Frontier Research Laboratory Program at the Korea Basic Science Institute.

References

1. C. Dekker, Phys. Today **52**, 22 (1999)
2. X. Duan, Y. Huang, Y. Cui, J. Wang, C.M. Lieber, Nature **409**, 66 (2001)
3. Y. Xia, P. Yang, Y. Sun, Y. Wu, B. Mayers, B. Gates, Y. Yin, F. Kim, H. Yan, Adv. Mater. **15**, 353 (2003)
4. C.N.R. Rao, F.L. Deepak, G. Gundiah, A. Govindaraj, Prog. Solid Chem. **31**, 5 (2003)
5. M.M. Thackeray, Prog. Solid State Chem. **25**, 1 (1997)
6. X. Chen, X. Li, Y. Jiang, C. Shi, X. Li, Solid State Commun. **136**, 94 (2005)
7. X. Wang, Y. Li, J. Am. Chem. Soc. **124**, 2880 (2002)
8. C.W. Na, D.S. Han, D.S. Kim, J. Park, Y.T. Jeon, G. Lee, M.-H. Jung, Appl. Phys. Lett. **87**, 142504 (2005)
9. W. Liu, G.C. Farrington, F. Chaput, B. Dunn, J. Electrochem. Soc. **143**, 879 (1996)
10. M. Matzapetakis, N. Karligiano, A. Bino, M. Dakanali, C.P. Raptopoulou, V. Tangoulis, A. Terzis, J. Giapintzakis, A. Salifoglou, Inorg. Chem., **39**, 4044 (2000)
11. M. Regulski, R. Przeniosło, I. Sosnowska, J.-U. Hoffmann, J. Phys. Soc. Japan **73**, 3444 (2004)
12. N. Ohama, Y. Hamaguchi, J. Phys. Soc. Japan **30**, 1311 (1971)
13. M. Regulski, R. Przeniosło, I. Sosnowska, D. Hohlwein, R. Schneider, J. Alloys Compd. **362**, 236 (2004)
14. E.G. King, J. Am. Chem. Soc. **76**, 3289 (1954)
15. R.W. Grant, S. Geller, J.A. Cape, G.P. Espinoza, Phys. Rev. **175**, 686 (1968)
16. S.H. Kim, B.J. Choi, G.H. Lee, S.J. Oh, B. Kim, H.C. Choi, J. Park, Y. Chang, J. Korean Phys. Soc. **46**, 941 (2005)
17. B. Boucher, R. Buhl, M. Perrin, J. Appl. Phys. **42**, 1615 (1971)
18. W.S. Seo, H.H. Jo, K. Lee, B. Kim, S.J. Oh, J.T. Park, Angew. Chem. **43**, 1115 (2004)
19. I. S. Jacobs, Chem. Solids **11**, 1 (1959)